Instabilities of the resonance attractor for spiral waves in an excitable medium

Vladimir S. Zykov,[1] On-Uma Kheowan,[1,2] Orapin Rangsiman,[2] and Stefan C. Müller[1]
[1]*Institut für Experimentelle Physik, Otto-von-Guericke-Universität, Universitätsplatz 2, D-39106 Magdeburg, Germany*
[2]*Department of Chemistry, Mahidol University, Rama 6 Road, Bangkok 10400, Thailand*
(Received 21 May 2001; published 16 January 2002)

During an experimental study of the resonance attractor for spiral waves in the light-sensitive Belousov-Zhabotinsky reaction, strong deviations of the attractor trajectories from circular orbits are observed if the time delay in the feedback loop becomes relatively long. A theory is developed that reduces the spiral wave dynamics under a long-delayed control to a higher order iterative map. Then the observed deviations are explained to be a result of instabilities appearing due to the Neimark bifurcation of the map. The theoretical predictions are in good agreement with the experimental data.

DOI: 10.1103/PhysRevE.65.026206 PACS number(s): 05.45.−a, 05.65.+b, 82.40.Bj, 47.54.+r

I. INTRODUCTION

Spiral waves rotating in an excitable medium are an important and characteristic example of dynamical spatiotemporal patterns. They have been observed in many nonlinear distributed systems as vortices of electrical activity in cardiac, tissue [1], CO oxidation fronts on platinum surfaces [2], or as chemical waves in the Belousov-Zhabotinsky (BZ) reaction [3,4]. Their dynamic behavior becomes especially rich and diverse when are subjected to parametric modulation of the excitability. This has been amply demonstrated in experiments with the light-sensitive BZ reaction [5–11]. In particular, the phenomenon of resonant drift attracts now a growing interest, because it provides an efficient way to control the dynamics of a spiral wave. Such a control is important for many applications, e.g., for the defibrillation of cardiac tissue [12–14].

The resonance attractor appears in excitable systems under a feedback control, when a pulsatory modulation of the excitability is synchronized with the passage of the wave pulses through a measuring point that can be arbitrarily chosen in the medium [3]. This feedback forcing results in a resonant drift of the spiral core around the measuring point. Recent experimental studies [11] reveal a complex structure of the attractor in that circular orbits of different sizes exist, which depend on the sign and the time delay in the feedback loop. The theory of the resonance attractor elaborated recently [15], reduces the dynamics of a spiral wave under one-channel feedback to a low dimensional iterative map. It predicts the existence of circular orbits and quantitatively describes their sizes.

However, the available experimental data [11] demonstrate pronounced deviations of the attractor orbits from the circular pathways, if the time delay is sufficiently long or the attractor size becomes sufficiently large. The reason for such deviations remains unknown, since they cannot be explained in the framework of the existing theory [15] that applies only to the case when the time delay τ is smaller than the rotation period T_0.

In this work we perform a systematic experimental study of resonance attractors under a long time delay in the feedback loop. A modified theory is developed to describe the dynamics of spiral waves under such a delayed control. The existence and the stability of the attractor orbits are analyzed. Finally, the obtained theoretical estimates are compared with the experimental data.

II. EXPERIMENTAL OBSERVATIONS OF THE RESONANCE ATTRACTOR

The experimental setup, in extension of that used in our previous studies [8,10,11], includes a petri dish with a thin (0.33 ± 0.02 mm) gel layer. The light-sensitive Ru $(bpy)_3^{2+}$ catalyst is immobilized in the gel at a concentration of 4.2 mM [16]. The BZ solution without catalyst is poured on top of the gel. After several minutes an equilibrium between liquid and gel is established and the following concentrations are reached: 0.2-M $NaBrO_3$, 0.17-M malonic acid, 0.39-M H_2SO_4, and 0.09-M NaBr. The experiments are carried out at a temperature of 22 ± 1 °C.

The petri dish is illuminated from below by a video projector (Panasonic PT I 555E) controlled by a computer via a frame grabber (Data Translation, DT 2851). The illuminating light is filtered with a bandpass filter (BC6, 310–530 nm). The pictures of the oxidation waves appearing in the gel layer are observed in transmitted light detected by a CCI camera (Hamamatsu H 3077) and digitized online for immediate processing by the computer. In parallel, the images from the camera are stored on a video recorder (Sony EVT 301).

A single spiral wave, which constitutes the initial condition for all the experiments, is created in the center of the dish by breaking a wave front with a cold intense light spot [11]. The tip of the spiral wave is defined as the intersection of contour lines ($0.6\times$amplitude) extracted from two consecutive frames of the digitized movie (time step 3.12 s). Its motion is followed automatically by the computer [9].

For the given background light intensity ($I_{bg}=0.12$ mW/cm^2) the tip moves on a circle with a diameter about 0.39 mm. The rotation period is $T_0\approx52$ s, the spiral wave pitch is $\lambda_0\approx1.98$ mm.

This rigid rotation of the spiral wave can be disturbed when applying a sequence of short light pulses. Each pulse induces a shift of the spiral wave core. The single shifts are

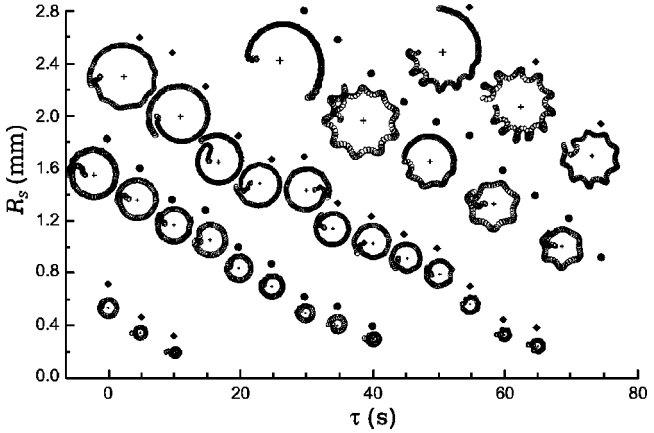

FIG. 1. Trajectories of the spiral wave tip under feedback control with time delay τ. The measured radius of the resonance attractor R_s is shown by diamonds (circles) for a negative (positive) sign of the light pulse with amplitude $A=0.08$ mW/cm^2. Strong deviations from a circular shape appear in the right upper corner of the (τ,R_s) plane.

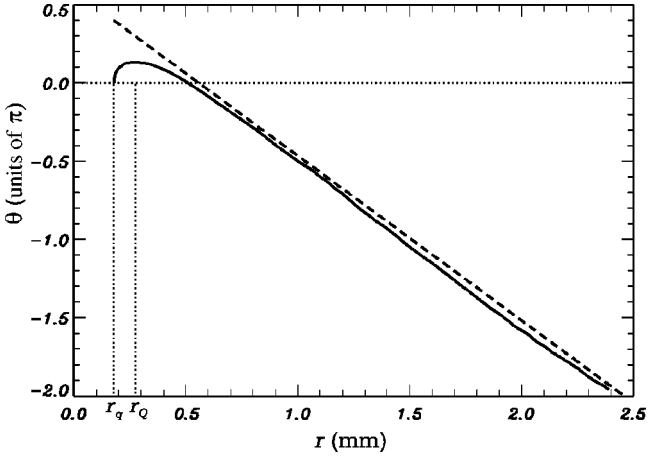

FIG. 2. Function $\Theta(r)$ specifying the experimentally observed shape of the spiral wave front. Radius r_q corresponds to the shortest distance between the core center and the contour line of the spiral wave attained at the spiral wave tip. Radius r_Q specifies the maximum of $\Theta(r)$ attained for the radius-vector tangent to the contour line. The dashed line represents the asymptotic behavior of $\Theta(r)$ for large r.

accumulated with time and cause a drift of the core [8,11]. In this work the light pulses (duration, 5 s) are created directly at the moment, when the wave front passes through a preselected measuring point, or after some time delay τ. Depending on the sign of the pulse the total illumination intensity is increased (positive pulse) or decreased (negative pulse) with respect to the background level.

In Fig. 1, a number of trajectories of a spiral wave tip are shown that represent experimental observations performed with different time delays in the feedback loop. For any value of τ several possible values of the orbit radius R_s exist. The radius depends on the pulse sign (cf. values given by diamonds and circles). However, even for a fixed pulse sign (say, a negative one) orbits with different radii were found depending on the initial distance between the spiral core and the measuring point. In order to reach an orbit with a larger radius, this distance should be longer and lie within the corresponding basin of attraction. An increase of τ results in a shrinking of the orbit radius, as reported earlier [9,11,15].

In the right upper corner of the Fig. 1 one can see strong deviations from a circular pathway. Small deviations of this kind have been already noticed in the experiments with the snail-shaped drift [11]. The results shown in Fig. 1 demonstrate that these deviations are reproducible and can be rather pronounced. They appear if the time delay in the feedback loop and/or the orbit radius become sufficiently large.

III. KINEMATICAL MODEL OF THE SPIRAL CORE DYNAMICS

We develop a simplified description of the spiral wave dynamics under one-channel feedback assuming that the unperturbed spiral rotates rigidly around a circular core with a constant angular velocity ω_0. The shape of its front can be specified in a polar coordinate system (Θ, r) with origin at the core center by a function $\Theta=\Theta(r)$, where $\Theta=0$ corresponds to the spiral wave tip. An example of this function obtained in our experiments is shown in Fig. 2.

Application of the pulse induces a displacement of the core center, as schematically shown in Fig. 3. In order to describe the displacement of the spiral core, we introduce another polar coordinate system (φ, R) centered at the measuring point (see Fig. 3). The distance to the core center R_i and the polar angle φ_i will specify the location of the core just before the pulse i is applied. In addition, angle α_i determines the location of the spiral tip at the same instant on its circular pathway around the core center. This angle is counted from the line connecting the core center and the measuring point. The induced displacement occurs in a di-

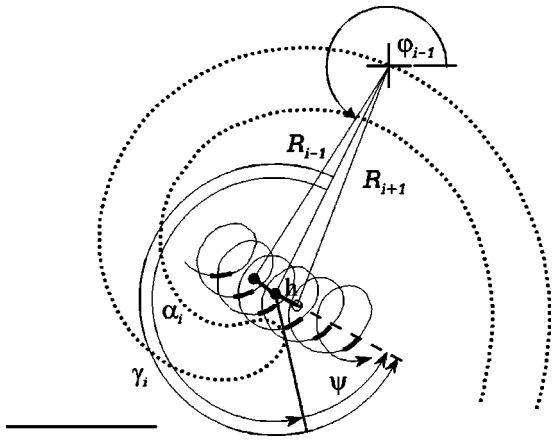

FIG. 3. Shift of the spiral wave core due to one pulse in a periodic sequence. The contour line (dotted) of a spiral wave is shown at the instant, when its front passes through the measuring point (cross). The thin looped line represents a part of the wave tip trajectory observed with $\tau=T_0$. Thick segments indicate application of light pulses. Locations of the core center just before the $(i-1)$th and ith pulse are shown as full circles. The core center after the ith pulse is shown as an open circle. Scale bar: 1 mm. (For details, see text.)

rection given by the angle γ_i measured with respect to the same line. The angle γ_i depends, of course, on the orientation of the rotating spiral wave given by the angle α_i and can be expressed as

$$\gamma_i = \alpha_i + \psi, \tag{1}$$

where the angle ψ is a constant that depends on the disturbance applied to the system [11].

If the absolute value of the induced displacement is h, the next location of the core is given by [15]

$$R_{i+1}^2 = R_i^2 + h^2 - 2R_i h \cos(\gamma_i), \tag{2}$$

$$\varphi_{i+1} = \varphi_i - \arcsin[(h/R_{i+1})\sin(\gamma_i)]. \tag{3}$$

These equations are a direct consequence of the cosine theorem-applied to the triangle with sides R_i, h, R_{i+1}.

If a pulse is applied just at the moment when the spiral front passes through the measuring point, the equation $\alpha_i = -\Theta(R_i)$ is valid [15] that follows from the definition of the function $\Theta(R_i)$. In the more general case of an arbitrary time delay the expression for α_i should be written as

$$\alpha_i = -\Theta(R_{i-k}) + \omega_0 \tau - k\delta\alpha - (\varphi_i - \varphi_{i-k}). \tag{4}$$

Here $k = [\tau/T_0]$ is the largest integer smaller than τ/T_0 and is equal to the number of full rotations made by the spiral wave during the delay time. This integer is as well the number of light pulses that have been applied to the system during the time interval τ. For $k=0$, Eq. (4) is identical to the expression for short τ [15]. The more complicated situation for $k=1$ is illustrated in Fig. 3 (for the particular choice $\tau = T_0$). During the trajectory loop numbered $(i-1)$ the wave front passes through the measuring point at the moment, when the angle α is equal to $-\Theta(R_{i-1})$. The new light pulse is not immediately generated, but with a time delay τ, during which the spiral continues to rotate with the angular velocity ω_0. While the angle α increases to $-\Theta(R_{i-1}) + \omega_0\tau$, an intermediate pulse is applied to the medium, as can be seen in Fig. 3. Generally speaking, the light pulses applied during the time interval τ can change the rotation velocity ω_0 of the unperturbed spiral. The effect of this perturbation has to be included in our consideration as a correction term $\delta\alpha$ (more generally $k\delta\alpha$, if $k \neq 1$). The last term in Eq. (4) appears due to the fact, that the angle α is counted from the radial direction φ_{i-1} for the $(i-1)$th loop, while for the ith loop the angle is counted from φ_i.

It is not difficult to generalize the above consideration carried out for $k=1$ in order to analyze the case of an arbitrary k. This generalization leads to Eq. (4).

The values h, ψ, $\delta\alpha$, and function $\Theta(r)$ can be measured experimentally. After this the system (1)–(4) is complete and describes the dynamics of the spiral core.

In order to simplify the analysis of system (1)–(4) let us assume that an applied light pulse changes the average rotation velocity only by a small amount $\delta\alpha \ll 1$. Moreover, Fig. 3 shows that $\varphi_{i-1} - \varphi_i \approx h/R_i$. Usually the ratio h/R_i is very small, e.g., for all orbits shown in Fig. 1, $h \ll R_i$ holds. Hence we can neglect the two last terms in Eq. (4) and write

$$\alpha_i = \omega_0 \tau - \Theta(R_{i-k}). \tag{5}$$

Now the map (1), (2), (5) describing the dynamics of R_i can be considered independently of Eq. (3) that specifies φ_i. This map has a number of equilibrium points R_s that do not depend on the value k and should satisfy the following equation:

$$\frac{h}{2R_s} = \cos\gamma_s. \tag{6}$$

Each equilibrium point corresponds to a circular orbit of radius R_s, if the whole map (1)–(3), (5) is considered, because the angle φ_i grows permanently with a constant velocity, determined by Eq. (3). Substituting Eqs. (1) and (5) into Eq. (6), the relation between the radius R_s of the attractor orbit and the time delay τ can be expressed as [11,15]

$$\frac{\tau}{T_0} = \frac{\Theta(R_s) - \arccos[h/(2R_s)] - \psi}{2\pi} + m, \tag{7}$$

or

$$\frac{\tau}{T_0} = \frac{\Theta(R_s) + \arccos[h/(2R_s)] - \psi}{2\pi} + m, \tag{8}$$

with m denoting a positive integer.

These expressions provide a quantitative estimate of the attractor radius R_s as a function of the delay τ in the feedback loop, if the parameters h, ψ, and the $\Theta(r)$ are determined experimentally [11,15]. In order to clarify the main features of the function $R_s(\tau)$ let us take into account that $h/(2R_s) \ll 1$ and assume an Archimedian shape of the spiral

$$\Theta(r) = \Theta_0 - 2\pi r/\lambda_0, \tag{9}$$

which is a linear approximation of the function $\Theta(r)$ for large r (see Fig. 2). Then Eq. (7) can be written as

$$\frac{R_s}{\lambda_0} = \frac{R_{00}}{\lambda_0} - \frac{\tau}{T_0} + m, \tag{10}$$

where R_{00} is the attractor radius corresponding to $\tau = 0$ and $m=0$ in Eq. (7). Under the same assumptions Eq. (8) reads

$$\frac{R_s}{\lambda_0} = \frac{R_{00}}{\lambda_0} - \frac{\tau}{T_0} + 0.5 + m. \tag{11}$$

Thus, for a fixed m the resonance attractor R_s is a decreasing function of the time delay τ as shown in Fig. 4. On the other hand, for each value of τ there are several possible attractor radii corresponding to different m. These results are both in agreement with the experimental observations (cf. Fig. 1). It is important to point out that, if dimensionless coordinates $(\tau/T_0, R_s/\lambda_0)$ are used, the entire structure of the resonance attractor shown in Fig. 4 is determined by only one parameter R_{00}/λ_0. This parameter depends on the characteristics h and ψ of the induced shift and can be estimated from Eq. (7) or measured directly.

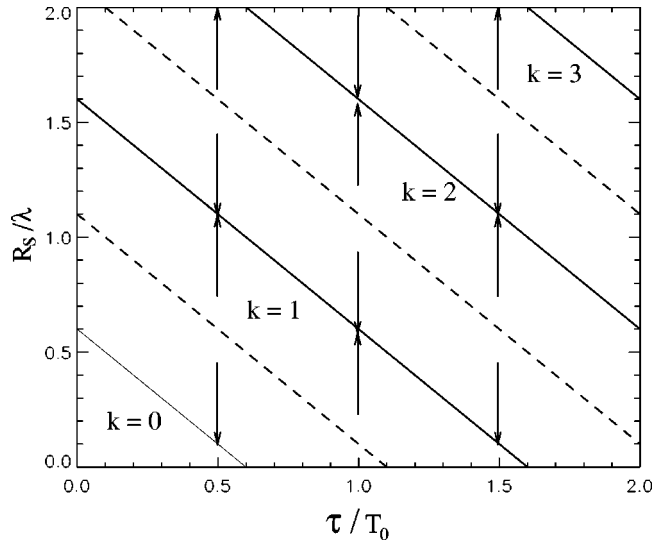

FIG. 4. Radius of the resonance attractor R_s vs time delay τ in the feedback loop. Solid and dashed lines are computed from the Eqs. (10) and (11), respectively, with $R_{00}/\lambda_0 = 0.6$. Arrows indicate directions of evolution of R_i within the basins of attracting orbits (solid) separated by unstable orbits (dashed). Within the basin of attraction $k = [\tau_\Sigma / T_0]$ remains constant.

IV. LINEAR STABILITY ANALYSIS

The stability of the orbits specified by Eqs. (7) and (8) is determined by the evolution of a small deviation δR_i near an equilibrium point, which obeys the following equation derived from the map (1), (2), (5),

$$\delta R_{i+1} - (1-\mu/2)\,\delta R_i + H\sqrt{1-\mu/4}\,\delta R_{i-k} = 0, \qquad (12)$$

where

$$\mu = \frac{h^2}{R_s^2}. \qquad (13)$$

H is a dimensionless shift written as

$$H = -h \left.\frac{d\Theta}{dr}\right|_{r=R_s}, \qquad (14)$$

for orbits described by Eq. (7) and as

$$H = h \left.\frac{d\Theta}{dr}\right|_{r=R_s}, \qquad (15)$$

for those described by Eq. (8). Under the assumption $\mu \ll 1$, the characteristic equation for the eigenvalues of Eq. (12) reads

$$\lambda^{k+1} - \lambda^k + H = 0. \qquad (16)$$

An equilibrium point of the discrete map (1), (2), (5) is stable under the condition $|\lambda| < 1$. Generally speaking, the characteristic equation (16) has $k+1$ roots, which can be found numerically for a given H. Figure 5 shows two examples of the displacement of the roots on the complex plane computed as a function of H. For $H = 0$ one root is always located at $\lambda = 1$, all others lie at $\lambda = 0$ [Fig. 5(a) and 5(b)]. With growing H the roots move through the complex plane and cross the unit circle, which corresponds to the Neimark

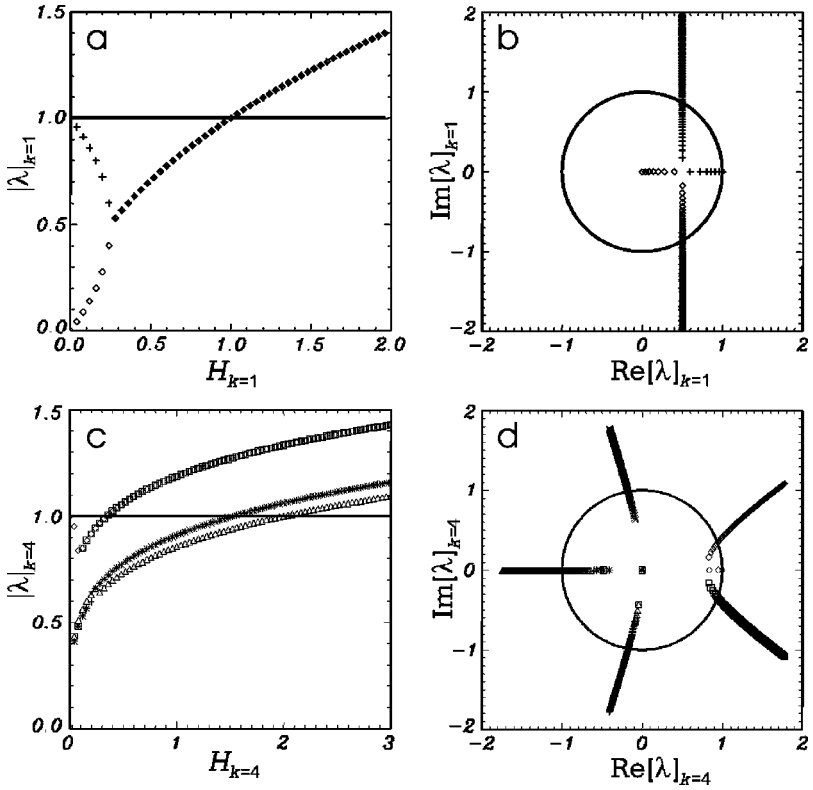

FIG. 5. Absolute values and locations of the roots of characteristic equation (16) on the complex plane vs the dimensionless shift H computed numerically for $k = 1$ [(a) and (b)] and for $k = 4$ [(c) and (d)].

bifurcation [17]. A sequence of Neimark bifurcations can be observed only in the map with $k \geqslant 3$ [cf. Figs. 5(c) and 5(d)], since two complex conjugated roots are involved in each of such a bifurcation.

Let us determine the critical values H_c of the dimensionless shift H corresponding to the Neimark bifurcation. Since at the bifurcation point $|\lambda|=1$ is valid, we can write

$$\lambda = \cos\beta + i\sin\beta, \tag{17}$$

where the value β is an unknown. Then Eq. (16) can be expressed as a system of two equations for H_c and β

$$\sin(k+1)\beta - \sin k\beta = 0, \tag{18}$$

$$\cos(k+1)\beta - \cos k\beta + H_c = 0, \tag{19}$$

which can be easily transformed to

$$2\cos\frac{2k+1}{2}\beta \sin\frac{\beta}{2} = 0, \tag{20}$$

$$-2\sin\frac{2k+1}{2}\beta \sin\frac{\beta}{2} + H_c = 0. \tag{21}$$

One possible solution of this system is the case $\sin\beta/2=0$,

$$H_c = 0; \quad \beta = 2\pi m. \tag{22}$$

Positive values of H_c correspond to the case $\cos[(2k+1)/2]=0$. Substituting this condition into Eq. (21) yields

$$H_c = 2\sin\left[\frac{\pi(4l+1)}{2(2k+1)}\right], \quad \beta = \frac{\pi(4l+1)}{2k+1}, \tag{23}$$

where $l=0,1,\ldots$ is an integer $l \leqslant k$. Since H_c is an increasing function of l, the minimal value of H_c found for $l=0$ describes the first Neimark bifurcation of the discrete map (1), (2), (5). The critical values obtained for $l>0$ specify higher Neimark or flip bifurcations.

Note that for all orbits shown in Fig. 1 the attractor radius R_s is larger than r_Q. It follows from Fig. 2 that at such large distances from the core the derivative $d\Theta/dr$ is negative. Consequently, for orbits described by Eq. (8) the dimensionless shift H is negative, as follows from Eq. (15) with $d\Theta/dr<0$. Analysis of Eq. (16) shows that at $H=0$ a cyclic fold bifurcation takes place and the attractor orbit becomes unstable for $H<0$. The unstable orbits play the role of the separatrices restricting basins of attraction for orbits described by Eq. (7). Figure 4 illustrates this statement for the case of an Archimedian shape of the spiral wave. Arrows in Fig. 4 show directions of variation of R_i for arbitrarily chosen initial distance between the measuring point and the spiral core. These directions corresponds to the performed stability analysis of the map (1), (2), (5), describing evolution of R_i under a fixed τ. Dashed lines indicates unstable orbits described in this case by Eq. (11). Solid lines specify attracting orbits.

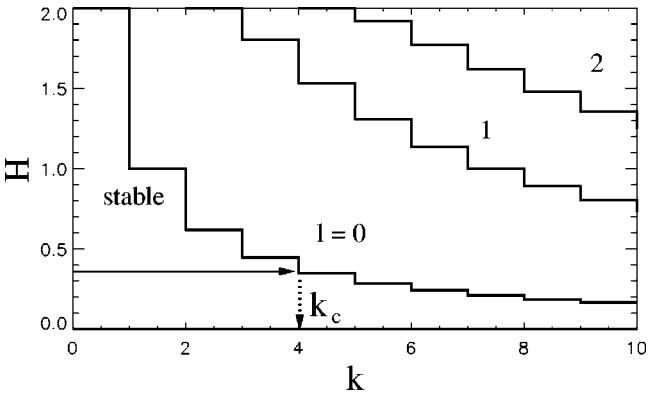

FIG. 6. Stability diagram for the map (1), (2), (5). Solids show the bifurcation boundaries on the (k,H) plane computed from Eq. (23) with $l=0$, 1, 2. Arrows illustrate the critical value k_c for a given dimensionless shift $H=0.38$.

These orbits [specified by Eqs. (7) or (10)] are stable, if H does not exceed a critical value H_c corresponding to the first Neimark bifurcation. The critical value depends on the order k of the map

$$H_c = 2\sin\left[\frac{\pi}{2(2k+1)}\right], \tag{24}$$

as follows from Eq. (20) with $l=0$. The corresponding stability diagram (Fig. 6) clearly shows that for an arbitrarily chosen H the stability of the equilibrium point is broken, if the value of k becomes larger than a critical value $k>k_c(H)$. Hence the attractor orbit cannot be stable, if the time delay τ exceeds a critical value $\tau > r_c = k_c T_0$, even if the shift $H>0$ is arbitrarily small. The boundaries with $l=1$ and $l=2$ shown in Fig. 7 correspond to higher bifurcations, which occur in the map (1), (2), (5) for larger values of H and/or k.

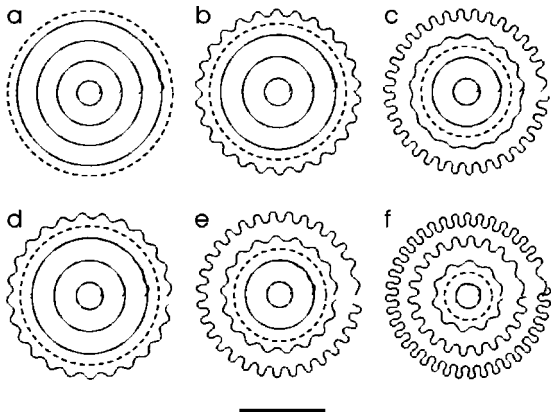

FIG. 7. Trajectories of a spiral core (solid) computed for the map (1)–(3), (5) with $\psi=0.157$ and $\Theta(r)$ corresponding to an Archimedian spiral (9) with $\lambda_0=50$ and $\Theta_0=0.64$. (a) $\tau=0$, $h=3$, (b) $\tau=0$, $h=4$, (c) $\tau=0$, $h=5$, (d) $\tau=T_0$, $h=3$, (e) $\tau=2T_0$, $h=3$, (f) $\tau=3T_0$, $h=3$. The dashed circle comprises the stability domain of radius R_c calculated from Eq. (32) with $R_{00}/\lambda_0=0.6$. Scale bar: 200.

V. EFFECT OF THE ATTRACTOR SIZE

As a consequence of the Neimark bifurcation periodic deviations from the circular orbit can be expected if $\tau > \tau_c$. In fact, such deviations are observed in the experiments with substantial delays in the control loop, as presented in Fig. 1. An important finding here is that the critical value of the time delay inducing this bifurcation decreases, when the attractor radius R_s grows. Indeed, under a negative pulse an instability is observed for $\tau = 74$ s and $R_s = 2.0$ mm, while for $R_s = 2.8$ mm it appears already at $\tau = 53$ s. In order to explain this fact, note that, if a spiral core is located at a distance R_s from the measuring point, it takes sometime for a wave to travel to this distance. This time is a natural property of the spatially distributed system under consideration and is equivalent, in some sense, to a time delay τ artificially introduced in the feedback loop.

Thus we have to take into consideration a ''total time delay'' τ_Σ that depends on both the time delay τ and the radius R_s of the attractor. A natural way to construct this dependence is to use the function $\Theta(r)$ describing the spiral shape (Fig. 2)

$$\tau_\Sigma = \tau - \Theta(R_s)/\omega_0 + \tau_0. \tag{25}$$

The term $-\Theta(R_s)/\omega_0$ specifies the time interval that is necessary for a spiral front to reach a point located at distance R_s from the spiral core. The integer k, which determines the order of the map (1)–(4), should be defined now as $k = [\tau_\Sigma / T_0]$.

The unknown constant τ_0 in Eq. (25) can be determined from the following consideration. Note that there is a relationship (7) between the attractor radius R_s and the time delay τ. Substituting Eq. (7) into Eq. (25) and taking into account that $h/(2R_s) \ll 1$ yields

$$\tau_\Sigma = mT_0 - \frac{\pi/2 + \psi}{\omega_0} + \tau_0. \tag{26}$$

Thus, the total time delay τ_Σ remains constant for all attractors described by Eq. (7) with a fixed m. Similarly, τ_Σ remains constant on a separatrix (8) between the two neighboring attractors. For instance, at the separatrix between attractors with $m=0$ and $m=1$ we get

$$\tau_\Sigma = \frac{\pi/2 - \psi}{\omega_0} + \tau_0. \tag{27}$$

At the separatrix the total delay time τ_Σ should be equal to T_0, since then it will separate two regions with $k=0$ and $k=1$. This condition is fulfilled if

$$\frac{\tau_0}{T_0} = 1 - \frac{\pi/2 - \psi}{2\pi} = 0.5 + \frac{\Theta(R_{00})}{2\pi}. \tag{28}$$

Finally, expression (25) determining the total time delay for an arbitrary spiral shape $\Theta(r)$ is written as

$$\tau_\Sigma = \tau - \frac{\Theta(R_s)}{\omega_0} + \frac{\Theta(R_{00})}{\omega_0} + 0.5T_0. \tag{29}$$

In the special case of an Archimedian spiral (9), this definition becomes particularly simple,

$$\frac{\tau_\Sigma}{T_0} = \frac{\tau}{T_0} + \frac{R_s}{\lambda_0} - \frac{R_{00}}{\lambda_0} + 0.5. \tag{30}$$

The values of $k = [\tau_\Sigma / T_0]$ computed with Eq. (30) are indicated on the (τ, R_s) plane of Fig. 4. k remains constant within a basin of attraction and jumps by 1 when crossing the separatrices. Hence, the critical value H_c, determined from the stability condition (24) is the same within a given basin of attraction, while particular values of τ and R_s can be different.

On the other hand, in accordance with the definition (30), the critical time delay τ_c depends on the attractor radius, in agreement with the experimental observation in Fig. 1. Within a basin of attraction, where $\tau_\Sigma / T_0 = k_c, \tau_c$ is expressed as

$$\frac{\tau_c}{T_0} = k_c - \frac{R_s}{\lambda_0} + \frac{R_{00}}{\lambda_0} - 0.5. \tag{31}$$

Similarly, the critical size R_c of the attractor should depend on the time delay τ and can be specified as

$$\frac{R_c}{\lambda_0} = k_c - \frac{\tau}{T_0} + \frac{R_{00}}{\lambda_0} - 0.5. \tag{32}$$

These expressions for τ_c and R_c are illustrated in Fig. 7, where the trajectories of the spiral core center for the map (1)–(3), (5) are computed. For these computations we used $T_0 = 6.9$, $\lambda_0 = 50$, $\psi = 0.157$, and assumed that the spiral shape is Archimedian, hence $d\Theta/dr = -2\pi/\lambda_0 = -0.126$.

Figure 7(a) shows four different trajectories corresponding to different initial conditions. In all cases the core center is rotating around the measuring point in the counterclockwise direction. The orbits closest to the measuring point (located at the symmetry center) started at $R_0 = R_{00}$ and $\varphi_0 = 0$. The other orbits started at $\varphi_0 = 0$ and $R_0 = R_{00} + n\lambda_0$, where the integer n is the number of the orbit counted from the smallest one. These trajectories are computed for $\tau = 0$, while the total delay time τ_Σ should be computed in accordance with Eq. (30) and will be proportional to the orbit number n, $\tau_\Sigma = (n + 0.5)T_0$. Consequently, the value of $k = [\tau_\Sigma / T_0]$ is simply equal to the orbit number. The computations were performed with $h = 3$ $(H = 0.38)$. In accordance with Eq. (24) one expects for this value of H that orbits with $k \geqslant 4$ are unstable (see also Fig. 6). The four trajectories shown in Fig. 7(a) correspond to the values $k = 0,1,2,3$ and are stable. Thus, there is a stability domain centered at the measuring point. The dashed curve in Fig. 7(a) shows the boundary of this domain with radius R_c calculated from Eq. (32) with $R_{00} = 0.6$. Figures 7(b) and 7(c) shows the trajectories computed for the same initial conditions, but for

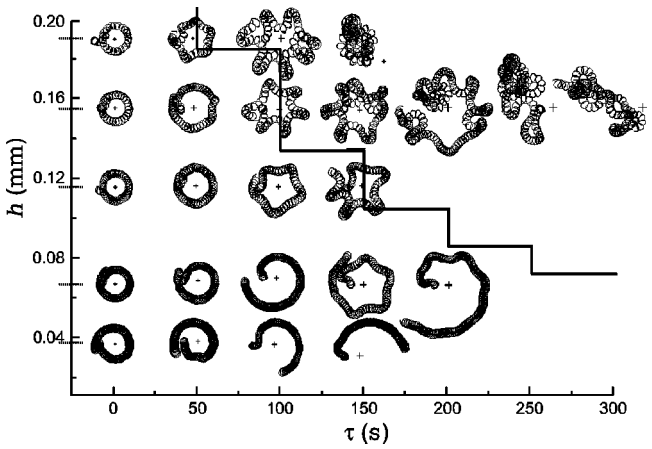

FIG. 8. Trajectories of the spiral tip observed for different time delay τ and shift h induced by light pulses of different intensities. The shifts marked by long bars on the h axis correspond to the following pulse amplitudes A: -0.2, -0.4, -0.6, -0.8 W/m^2 with pulse duration 5 s (from bottom to top), and $A=-0.8$ W/m^2 with pulse duration 6 s for the upper bar. The boundary of the Neimark bifurcation computed according to Eq. (33) is shown as a solid line.

$H=0.5$ and $H=0.63$, respectively. In the first case $k_c=3$ and in the second one $k_c=2$. The size of the stability domain R_c becomes progressively smaller. The orbit with $k=3$ loses its stability first [Fig. 7(b)], and subsequently the two orbits with $k=3$ and $k=2$ become unstable [Fig. 7(c)].

Schemes (d)–(f) of Fig. 7 illustrate the effect of the time delay τ on the orbit stability. All corresponding computations were performed for fixed $H=0.38$. If $\tau=T_0$, the stability domain computed with Eq. (32) is so small, that the orbit with $k=3$ becomes unstable [Fig. 7(d)]. Further growth of τ results in a destabilization of the orbits with $k=2$ [Fig. 7(e)] and $k=1$ [Fig. 7(f)].

This shows that computations with the discrete map (1)–(3), (5) are in good agreement with the analytical estimates (24) and (32). These computations illustrate also that the attractor of larger size becomes unstable for shorter time delay in qualitative agreement with the experimental data shown in Fig. 1.

VI. EXPERIMENTAL STUDY OF THE STABILITY BOUNDARY

An experimental study has been performed with the goal to allow a direct comparison between the theoretical predictions and the measurements. In Fig. 8 a number of different trajectories are shown that correspond to the experiments carried out with different time delay τ and at different intensities of the light pulse. The increase of pulse intensity results in a larger shift h specified as the ordinate of Fig. 8. As a qualitative result in this (τ,h) coordinate system one sees that the attractor trajectory becomes unstable, if τ and/or h are sufficiently large. To perform a quantitative comparison with the model results, the boundary of the Neimark bifurcation is added to Fig. 8 (cf. Fig. 6). Here the critical values of the time delay τ_c are computed using Eq. (31) with $R_s=R_{00}+0.5\lambda_0$ yielding

$$\frac{\tau_c}{T_0}=k_c-1. \tag{33}$$

The critical values of h are computed using Eqs. (24) and (14) with $d\Theta/dr=-2\pi/\lambda_0=-3.3\ \mathrm{mm}^{-1}$, which corresponds to the observed shape of the spiral front shown in Fig. 2.

The theoretically determined boundary is in good quantitative agreement with the experimental observation of stable and unstable attractor orbits. Indeed, all stable trajectories lie below the instability boundary. For several experiments, however, an instability appeared earlier, i.e., below the theoretically predicted bifurcation line. This indicates that our model is an approximation (a good one) derived under several simplifying assumptions and cannot be absolute.

VII. CONCLUSION

In summary, the systematic study of the spiral wave dynamics under a one-channel feedback control demonstrates an unexpectedly rich variety of attractor trajectories observed for a long time delay. A modified theory of the spiral core dynamics has been developed that reduces the observed behavior to an iterative map, the order of which depends on the time delay. In the framework of this model the observed deviations from the circular shape of core trajectories are found to be a consequence of the Neimark bifurcation. A linear stability analysis yields an analytical expression for the instability boundaries. The main qualitative result of the study is that for a given intensity of the light pulse the stability of the resonance attractor is determined by the total delay time τ_Σ that depends on the time delay τ in the feedback loop and on the attractor size R_s [see definition (29)]. The resonance attractor becomes unstable, if τ_Σ/T_0 exceeds a critical value k_c (e.g., see Figs. 6 and 7). These model predictions are in quantitative agreement with both numerical computations of the map and with experimental observations as shown in Fig. 8.

Spiral wave dynamics under a long-delayed control constitutes as a broad and prospective field for both theoretical and experimental studies. From a theoretical point of view the resonance attractor represents a natural example of a nonlinear dynamical system with multiple steady states and a cascade of bifurcations. Having in mind such an important application as the defibrillation of cardiac tissue, an investigation of the basic properties of the long-delayed control of spiral waves remains a most interesting challenge for future work.

ACKNOWLEDGMENTS

O.K. thanks the Deutscher Akademischer Austauschdienst (DAAD) and Research Program in Chemistry funded by the Royal Thai Government for financial support.

[1] J. M. Davidenko, A. V. Pertsov, R. Salomonsz, W. Baxter, and J. Jalife, Nature (London) **355**, 349 (1992).
[2] S. Jakubith, H. H. Rotermund, W. Engel, A. von Oertzen, and G. Ertl, Phys. Rev. Lett. **65**, 3013 (1990).
[3] A. T. Winfree, Science **175**, 634 (1972).
[4] S. C. Müller, T. Plesser, and B. Hess, Science **230**, 661 (1985).
[5] K. I. Agladze, V. A. Davydov, and A. S. Mikhailov, Pis'ma Zh. Eksp. Teor. Fiz. **45**, 601 (1987) [JETP Lett. **45**, 767 (1987)].
[6] O. Steinbock, V. S. Zykov, and S. C. Müller, Nature (London) **366**, 322 (1993).
[7] M. Braune and H. Engel, Chem. Phys. Lett. **211**, 534 (1993).
[8] S. Grill, V. S. Zykov, and S. C. Müller, Phys. Rev. Lett. **75**, 3368 (1995).
[9] S. Grill, V. S. Zykov, and S. C. Müller, J. Phys. Chem. **100**, 19 082 (1996).
[10] D. M. Goldschmidt, V. S. Zykov, and S. C. Müller, Phys. Rev. Lett. **80**, 5220 (1998).
[11] O. Kheowan, V. S. Zykov, O. Rangsiman, and S. C. Müller, Phys. Rev. Lett. **86**, 2170 (2001).
[12] K. Hall, D. J. Christini, M. Tremblay, J. J. Collins, L. Glass, and J. Billette, Phys. Rev. Lett. **78**, 4518 (1997).
[13] E. V. Nikolaev, V. N. Biktashev, and A. Holden, Chaos, Solitons Fractals **9**, 363 (1998).
[14] A. Panfilov, S. C. Müller, V. S. Zykov, and J. P. Keener, Phys. Rev. E **61**, 4644 (2000).
[15] A. Karma and V. S. Zykov, Phys. Rev. Lett. **83**, 2453 (1999).
[16] T. Yamaguchi, L. Kuhnert, Zs. Nagy-Ungvarai, S. C. Müller, and B. Hess, J. Phys. Chem. **95**, 5831 (1991).
[17] The Neimark bifurcation is a discrete-time analogue of the Hopf bifurcation appearing in continuous systems; see e.g., J. M. T. Thompson and H. B. Stewart, *Nonlinear Dynamics and Chaos* (Wiley, Chichester, 1997).